이학석사 학위논문

리튬이온배터리 음극 소재인 Zinc borate의 탄소와 LATP의 하이브리드 코팅을 통한 높은 C-rate에서의 안정적인 사이클링

A hybrid coating of carbon and LATP
enabling stable cycling
at high C-rates in Zinc borate
as anode for Li-ion batteries

울산대학교 대학원

화학과

김정인

A hybrid coating of carbon and LATP enabling stable cycling at high C-rates in Zinc borate as anode for Li-ion batteries

지도교수 이 영 일

이 논문을 이학석사학위 논문으로 제출함

2024년 02월

울산대학교 대학원

화학과

김정인

김정인의 석사학위 논문을 인준함

심사위원 이영일 (인)

심사위원 하지원 (인)

심사위원 이동호 (인)

울 산 대 학 교 대 학 원

2024년 02월

English Abstract

The anode material is a crucial component of a lithium-ion battery (LIB) as it determines the battery's charging rate and lifetime. Additionally, the battery's energy density improves with the number of lithium ions it can store. Therefore, it is imperative to identify an anode material that meets these requirements and complements the strengths and weaknesses of commercialized carbon and silicon.

In this study, zinc borate was synthesized due to its low cost and high theoretical capacity of 512.5 mAh g^{-1}. To overcome the problem of borate's susceptibility to oxidation, it was coated with carbon and solid electrolyte, LATP. This was done to enhance the permeation of Li ions.

The structural and morphological properties of $Zn_3(BO_3)_2$@C_LATP were confirmed by X-ray diffraction (XRD) and scanning electron microscopy (SEM-EDX) equipped with energy dispersive X-ray analysis spectroscopy. The electrochemical performance was tested using a galvanostatic automatic battery cycler in the potential range of 0.05-3.0 V with CR2032 coin cells. The results showed that $Zn_3(BO_3)_2$@C and $Zn_3(BO_3)_2$@C_LATP exhibited better capacity and cycling performance compared to the bare material. Specifically, $Zn_3(BO_3)_2$@C_LATP with a hybrid coating can be considered a reliable anode material that maintains stable capacity even at high charge rates.

국문 초록

리튬이온 배터리(LIB)의 음극재는 배터리의 충전 속도와 수명을 결정하는 중요한 소재이다. 또한, 리튬 이온을 많이 저장할 수 있을수록 전지의 에너지 밀도 향상에 도움을 줄 수 있다. 앞선 조건을 만족하며, 상용화된 카본과 실리콘의 장점 및 단점을 보완할 수 있는 음극재 연구가 필수적이다.

본 연구에서는 가격이 저렴하고, 512.5 mAh g^{-1}의 높은 이론 용량을 갖는 등의 장점을 갖는 Zinc borate를 합성하였다. 또한 산화되기 쉬운 borate의 단점 보완을 위한 탄소(C) 코팅과 Li 이온의 투과를 촉진시키기 위해 고체 전해질인 LATP의 코팅도 동시에 진행하였다.

Zn3(BO3)2@C_LATP의 구조 및 형태학적 특성은 X-선 회절 장치(XRD) 및 에너지 분산 X-선 분석 분광기가 장착된 주사 전자 현미경(SEM-EDX)을 이용하여 확인되었다. 전기화학적 성능은 CR2032 코인셀로 0.05-3.0 V의 전위 범위에서 galvanostatic automatic battery cycler를 이용하여 평가되었다. 그 결과, bare한 물질과 비교하였을 때, $Zn_3(BO_3)_2$@C와 $Zn_3(BO_3)_2$@C_LATP가 더욱 우수한 용량 및 사이클링 성능을 나타냄을 확인할 수 있었다. 특히 하이브리드 코팅을 한 $Zn_3(BO_3)_2$@C_LATP는 높은 충전 속도에서도 안정적인 용량을 유지할 수 있는 음극재라고 판단할 수 있다.

Contents

List of tables

List of figures

1. Introduction

1.1 The introduction of Li-ion batteries

A battery is a device that converts chemical energy from electrode materials into electrical energy through electrochemical reactions.[1] Batteries are classified as primary or secondary based on their charge/discharge capabilities.[2] Primary batteries, such as alkaline, mercury, and lithium batteries, can only be used once during their lifetime.[3] Secondary or rechargeable batteries, such as nickel-cadmium (Ni-Cd) batteries, nickel-metal hydride (Ni-MH) batteries, lithium-ion (Li ion) secondary batteries, and lithium-ion polymer secondary batteries, are batteries that can be recharged and used repeatedly for a long period of time.[4-7]

Due to its low reduction potential and small ionic radius, Li is the lightest metallic element and possesses inherent beneficial properties that give LIBs a significant advantage.[8] LIBs are highly attractive as a promising energy storage technology due to their high energy density, low self-discharge characteristics, near-zero memory effect, and long lifetime.[9] In the automotive industry, high-energy density LIBs have been recently considered as an ideal power source for electric vehicles (EVs) and hybrid electric vehicles (HEVs).[10-11]

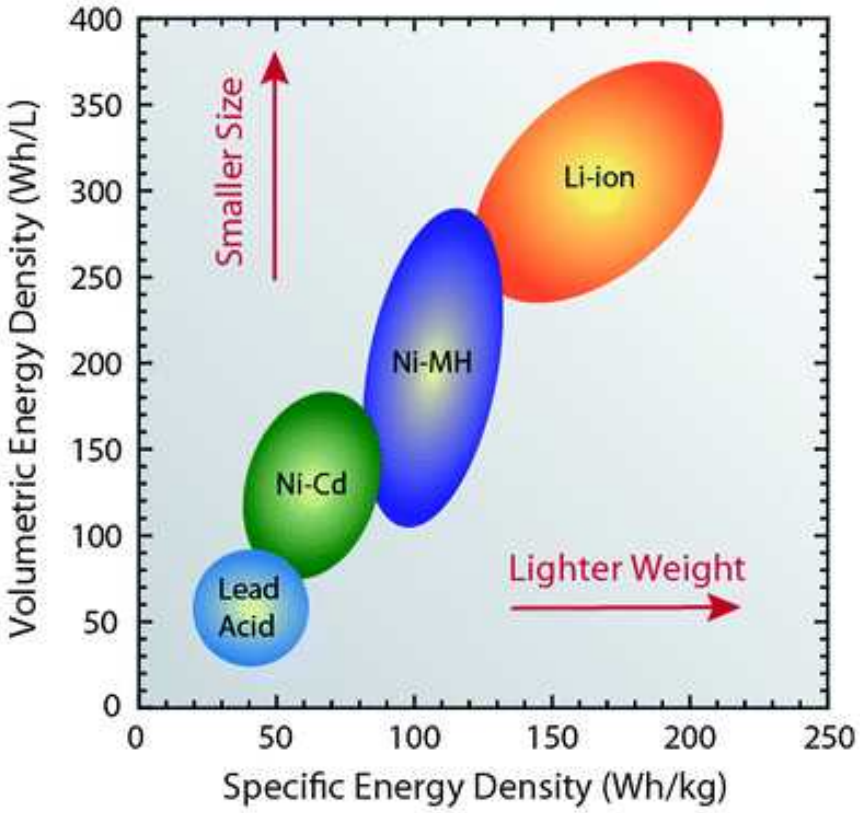

Figure 1.1 Energy density comparison of size and weight.[12]

Battery type	Power density /(w/kg)	Energy density /(w • h/ kg)	Unit voltage /V	Cycle life /time	Cost /[$/(kw • h)	Environmental protectio
Lead-acid batteries	200 ~300	35~40	2.0	300 ~500	75~150	Pollution
Nickel-cadmium batteries	150 ~350	40~60	1.2	500 ~1000	100~200	Serious pollution
NiMH batteries	150 ~300	60~80	1.2	500 ~1000	230~500	No pollution
Lithium ion battery	250 ~450	90~160	3.6	600 ~1200	120~200	No pollution
Vanadium flow battery	150 ~300	16~33 (w · h/L)	1.2	13000	150~450	No pollution

Table 1. Comparison of performance parameters of different types of secondary batteries.[13]

1.2 The principles and components of Li-ion batteries

For a cell to function as a rechargeable battery, its cathode and anode must have a structure that enables repeated charging and discharging.[14] This necessitates easy insertion and removal of ions from the electrodes, stable electrode structure during these processes, and an electrolyte that facilitates ion transfer. **Figure 1.2** shows a schematic of a typical lithium-ion battery.[15]

A lithium-ion battery is a device that converts chemical energy into electrical energy by moving lithium ions between the cathode and anode through an electrolyte and participating in a redox reaction at the electrodes.[1] The cathode and anode provide the sites for the major redox reactions in the energy conversion process, while the electrolyte provides a pathway for the movement of lithium ions. The separator also provides insulation to prevent the anode and cathode from touching directly.[16]

During charging, lithium ions move from the cathode material's crystal structures through the separator to the anode, while the generated electrons are transferred to the anode through external conductors.[17] During discharging, the lithium ions move back through the separator to the cathode, and the electrons move to the cathode as well. This process generates electricity. The insertion of lithium ions into the crystal structure of the cathode or anode material is called intercalation.[18] If a $LiMO_2$ (M = transition metal) oxide such as $LiCoO_2$ is used as the cathode and graphite is used as the anode, the above reaction can be represented as follows.

Cathode: $Li_{1-x}MO_2 + xLi^+ + xe^- \rightarrow LiMO_2$

Anode: $Li_xC_6 \rightarrow C_6 + xLi^+ + xe^-$

Full Cell Reaction: $Li_{1-x}MO + Li_xC_6 \rightarrow LiMO_2 + C_6$

In detail, the anode consists of an active material, a conductive additive, a binder, and a current collector. The active material is mainly lithium transition metal oxide, although other compounds such as phosphate and silicate are also used.[19] Highly conductive amorphous carbon particles such as carbon black are mainly used as conductive additives, and are used to improve the speed of electrode reaction by increasing electronic conductivity between cathode material particles.[20] The current collector gathers the flow of electrons produced during charge and discharge and connects them to the external conductors. Aluminum foil is primarily utilized for the anode. PVDF and other polymer materials are commonly used for the binder, which is used to secure the bonding force between the anode material particles and the bonding force between the anode material particles and the collector.[21]

The anode, like the cathode, contains a carbon black-based conductive additive and a polymer binder, and copper foil is often used as the electrolyte for the anode.[22] Copper foil is often used as a collector for the anode due to aluminum's tendency to react with lithium at the anode's operating potential and form an alloy. Copper, on the other hand, remains stable and does not participate in redox reactions at the anode's operating potential.[22] The anode material, along with the cathode, is crucial for energy storage. Carbon-based materials, such as graphite, are commonly utilized as anode

materials. However, new materials, including soft carbon and hard carbon, have been introduced for use in electric vehicle batteries.[23]

The electrolyte is a lithium salt dissolved in a carbonate-based organic solvent, providing a pathway for the lithium ions. The separator is a porous membrane made of polyolefins, such as polyethylene, which prevents electrical short circuits.

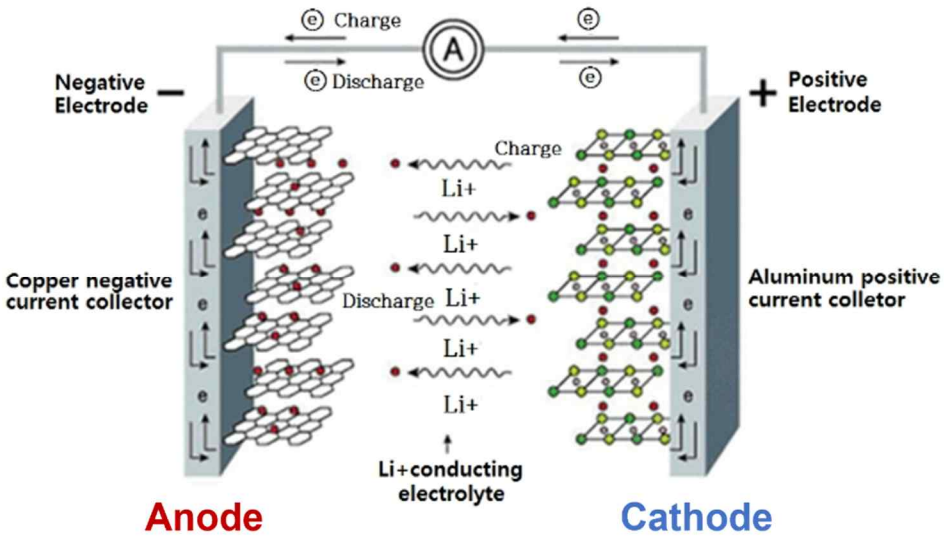

Figure 2.2 Schematic diagram of a typical Li-ion battery and the electrochemical charge-discharge process of LIBs.[15]

1.3. Anode materials

The anode is a crucial component of the battery as it reversibly absorbs and releases lithium ions from the cathode, allowing current to flow through the external circuit. It plays a significant role in determining the charging rate and lifetime of the battery. Anode materials must possess high energy density, lifetime characteristics, and charge/discharge efficiency. High energy density necessitates high capacity per weight or volume and low operating potential.[24]

Currently, carbon-based materials are the anode materials used in LIBs. These materials do not contain lithium, but they provide a space for lithium ions to exist and are connected by external wires to facilitate the acceptance or transfer of electrons. These carbon-based materials can be broadly categorized into graphitic and amorphous carbon.

Graphite is divided into two types: natural and artificial.[25] Natural graphite is less expensive than artificial graphite and has a higher capacity for storing lithium ions. However, due to high demand, natural graphite alone cannot meet the needs of the market. Therefore, there is a need to develop high-performance artificial graphite to replace it. Artificial graphite has a more stable crystal structure than natural graphite, resulting in a lifespan two to three times longer than natural graphite. It is created by applying high heat of over 2500 ℃ to form the graphite crystal structure.[26] However, the cost is high due to the use of high heat.

Amorphous carbon systems are classified into two types: soft carbon

(graphitizable carbon), which can be graphitized at high temperatures, and hard carbon (non-graphitizable carbon), which is difficult to graphitize. Hard carbon is suitable for high-power applications due to its low crystallinity and easy access to lithium ions. It is expected to be used in fields that require fast charging characteristics.[27]

Silicon is an excellent anode material for use in LIBs due to its large weight and volume capacity of about 3500 mAh g^{-1}, low cost, and abundance on Earth.[28] Additionally, it poses no stability risk compared to graphite electrodes due to its low working potential. However, a major drawback of silicon is its tendency to undergo significant volume changes during the lithium-ion insertion/extraction process. For instance, at 415 ℃, $Li_{22}Si_5$($Li_{4.4}Si$) exhibits a high lithium storage capacity of 4200 mAh g^{-1}. However, it also undergoes a significant volume expansion of approximately 310 %.[29] As a result, the actual capacity of a practical Si anode is much lower than the theoretical value. Research is currently being conducted to address this issue, such as forming complexes with carbon.

Anode	Benefits	Limitations
Carbon	1. Electronic conductivity is high 2. Commendable hierarchical structure 3. Inexpensive resources which are also abundant	1. It has a low specific capacity 2. It has a low rate capacity 3. It is associated with safety risks
Silicon	It has a very high specific capacity (3579 mAh g^{-1})	1. Very large change in volume (300%)

Table 2. The benefits and drawbacks of different anode materials for lithium-ion batteries.[30]

1.3.1 Solid electrolyte interphase

When a battery is charged, lithium ions migrate to the negative electrode, forming a thin solid film on its surface. This film is known as the solid electrolyte interphase (SEI), and is created as the materials in the electrolyte are first electrolyzed.[31] The SEI is formed mostly at low electromotive forces (0.0-0.8 V vs. Li metal).

The SEI prevents further degradation of the electrolyte, which serves as the pathway for the lithium ions to move.[31] It acts as a separator, reducing the chance of an internal short and allowing only the lithium ions to move through the electrolyte.

It is important to maintain an appropriate amount of SEI to ensure optimal battery performance. If there is an excess of SEI, it can impede the flow of electrons and lithium ions. In irregular cases, the migration of lithium ions towards the thinner side of the SEI can increase current density and create an electron avalanche effect, ultimately reducing the battery's lifetime.[32] Additionally, the SEI can be consumed as a reactant, leading to a loss of capacity and a decrease in the total number of lithium ions. To ensure SEI performs effectively, it is crucial to create a suitable film. Therefore, electrolyte additives like fluoroethylene carbonate (FEC), vinylene carbonate (VC), and others are occasionally included.[33-41]

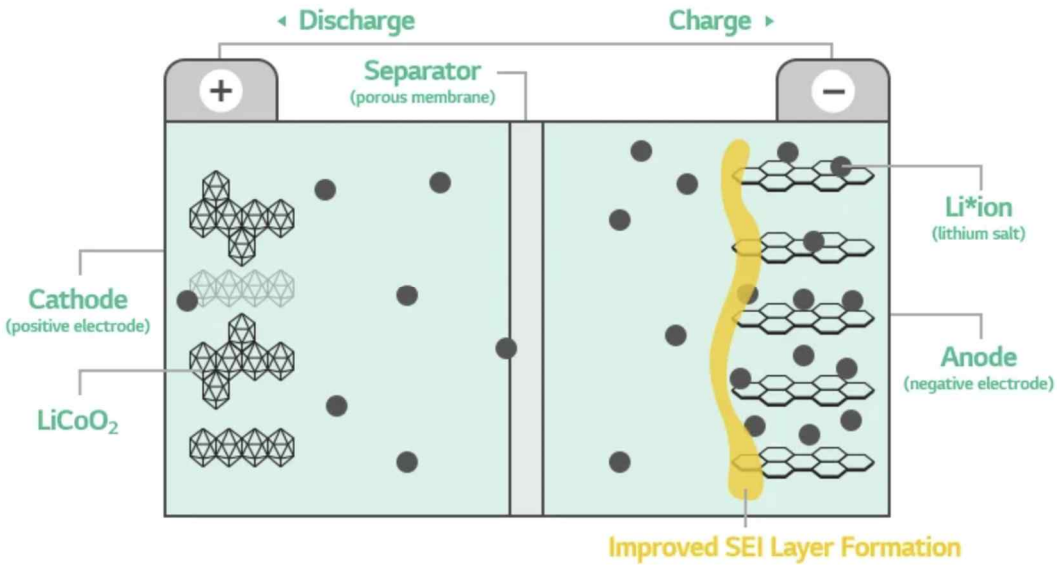

Figure 1.3 Schematic presentation of the SEI formation on anode.

1.4 Zinc borate

Inorganic borate has been studied as an electrode material for cathodes and anodes due to its inexpensive and stable BO_3^- triangle polyanion-type structure. The BO_3^- triangle is strongly covalently bonded to O and has a three-dimensional open channel, providing a good diffusion pathway for lithium ions. Additionally, it is relatively stable against volume changes during charge and discharge.

$Zn_3(BO_3)_2$ is a promising anode candidate due to its low cost, non-toxicity, and environmental friendly properties, as well as its high theoretical capacity of 512.5 mAh g^{-1}. It also has the advantage of being able to accommodate alkali metal ions such as Li and Na.

In this study, we synthesized and evaluated zinc borate based on these advantages. Additionally, we attempted to compensate for borate's weakness to moisture and air by applying a carbon coating. In addition, solid electrolyte, $Li_{1.3}Al_{0.3}Ti_{1.7}(PO_4)_3$ (LATP) was coated to act as a barrier between the active material and the electrolyte. This protects the active material and facilitates the permeation of Li ions.

In this experiment, we used FEC as an electrolyte additive to improve cycling stability. The use of FEC as an electrolyte additive resulted in improved cycling stability due to the formation of the SEI layer.[37] This decision was based on recent literature that suggests EC-based electrolytes alone are insufficient. FEC breaks C-F bonds and forms LiF[41], which in turn forms a protective coating known as SEI on the electrode material.

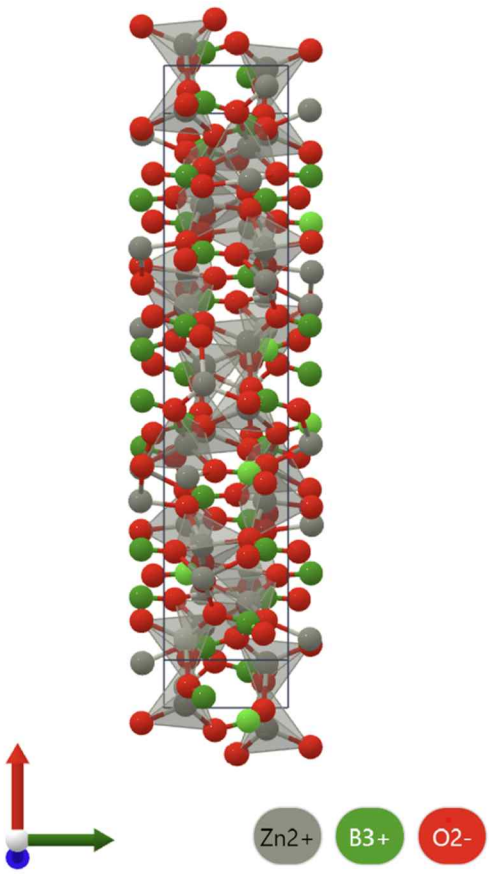

Figure 1.4 Structure of zinc borate.

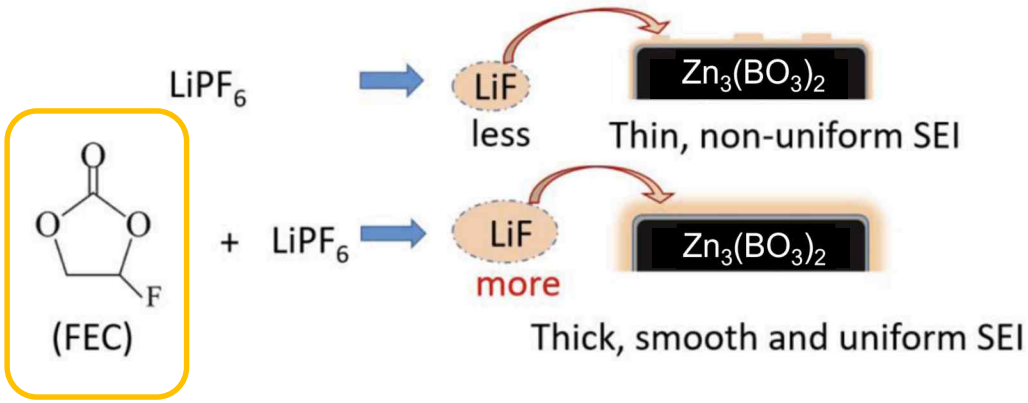

Figure 1.5 Schematic representing SEI layer formation on the anode materials.

2. Experimental

2.1 Synthesis

Zinc borate was synthesized by a solid-state reaction method. First, $Zn_3(BO_3)_2$ was synthesized, followed by coating with C and LATP. The precursors used for $Zn_3(BO_3)_2$ were $Zn(CH_3CO_2)_2$ (Aladin, ≥ 99%) and H_3BO_3 (Kanto, ≥ 99.5%). Li_2CO_3 (Aldrich, ≥ 99.0%), $AlOH(OOCCH_3)_2$ (Aldrich, ≥ 100.0%), TiO_2 (Aldrich, ≥ 100.0%), and $NH_4H_2PO_4$ (Junsei, ≥ 99.5%) were used as precursors for LATP, while ground sucrose (Junsei, ≥ 100%) was used as a source of carbon.

To synthesize $Zn_3(BO_3)_2$, various reagents were dissolved in acetone and planetary milled with 200 g of zirconia balls for 3 hours. The resulting precursor was dried in an oven at 80 °C for about 12 hours and then ground to uniformity using an agate mortar and pestle. The prepared $Zn_3(BO_3)_2$ precursor was treated at 370 °C for 1 hour and sintered at 500 °C for 2 hours under pure Ar gas in a tube furnace at a rate of 5 °C min^{-1}. Finally, it was cooled to room temperature to form bare $Zn_3(BO_3)_2$.

To coat LATP, bare $Zn_3(BO_3)_2$ and 7.5 wt.% LATP are ball milled with the same conditions as before and then treated in a tube furnace at 700 ℃ for 5 hours. Similarly, for coating C, 5 wt.% of finely ground sucrose and $Zn_3(BO_3)_2$ are subjected to the same process. Additionally, for the hybrid coating, LATP is coated first, followed by the carbon coating.

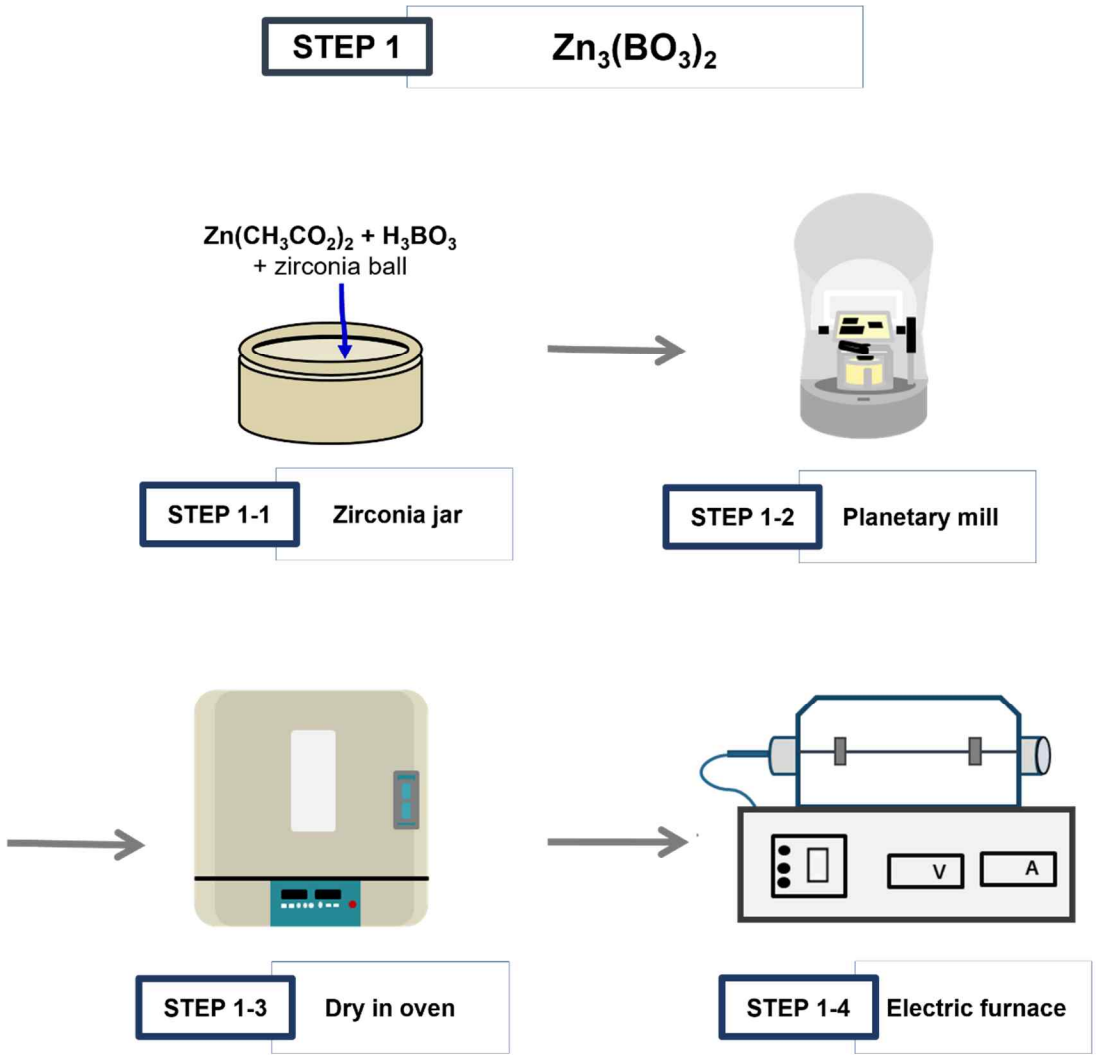

Figure 2.1 First-step synthetic procedures of $Zn_3(BO_3)_2$ by solid-state reaction.

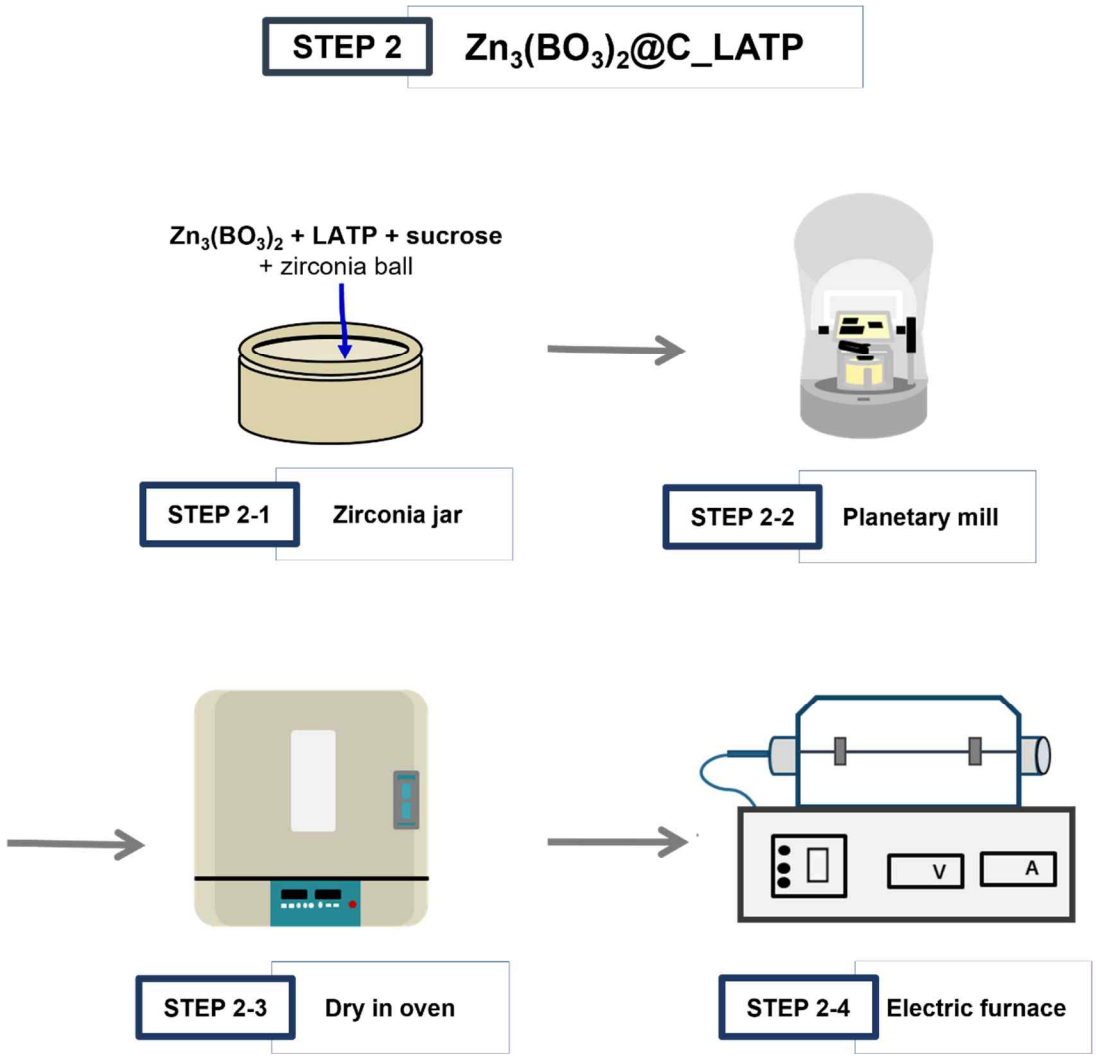

Figure 2.2 Second-step synthetic procedures of $Zn_3(BO_3)_2$ by solid-state reaction.

2.2 Characterization of the materials

The crystal structure and phase of the four synthesized materials were confirmed using a X-ray diffractometer (Rigaku Ultima IV, Japan) with Cu Ka radiation (λ=1.5406 Å). XRD patterns were obtained in the 2θ range from 10 to 80° at 50 kV and 40 mA in continuous scan mode at a rate of 2° min^{-1}.

The elemental composition of the four synthesized materials was investigated using field emission scanning electron microscope (FE-SEM, JEOL JSM6500F, Japan) combined with energy dispersive X-ray spectrometry (EDX, Oxford Instrument X-Max, UK). The materials synthesized were spread on the surface of carbon tape, coated with Pt using an auto sputter coater, and used as SEM samples.

2.3 Electrochemical measurements

The slurry for the anode electrode was composed of 74 wt.% of active material, 20 wt.% of Super P as a conductive additive, and 3 wt.% each of Na-CMC and PAA as binders. To control the viscosity, 2.5 ml of ethanol was added during the preparation of the slurry using a planetary mill. The slurry was then cast onto Cu foil using a doctor blade and dried overnight in a vacuum oven at 80 ℃. Finally, it was rolled into a uniform thickness using a roll press.

To perform the electrochemical analysis, a CR2032 coin cell was assembled in a glove box filled with argon gas. The counter electrode was Li metal foil, and the separator was a Celgard-2400 porous polypropylene membrane. The electrolyte used was 1.0 M LiPF6 in EC/DMC (ethylene carbonate/dimethyl carbonate) with a volume ratio of 1:1, containing 13 wt.% FEC electrolyte additive.

The electrochemical performance of the cells was evaluated at room temperature using a galvanostatic automatic battery cycler (WonA Tech WBCS 3000, Korea). The cells were tested within the voltage range of 0.05 to 3 V. To evaluate the cycling performance, measurements were taken within the current range of 0.05 to 2 A g^{-1}. To measure long cycling, measurements were made at a rate of 1 A g^{-1} for 800 cycles. Furthermore, measurements were performed at rates of 2, 5, and 10 A g^{-1} with 50 cycles at each rate to determine performance at additional high rates.

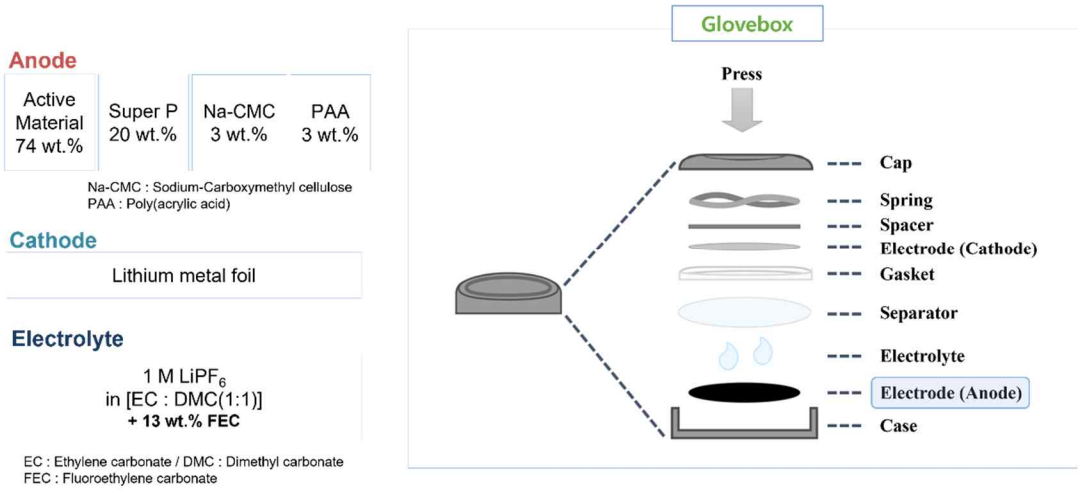

Figure 2.3 Schematic representation of CR2032 coin cell manufacturing process.

3. Results and Discusstion

3.1 Structural identification

3.1.1 X-ray diffraction (XRD) patterns of synthesized active materials

X-ray diffraction is a technique used to determine the phase and crystal structure of a solid sample by analyzing the diffraction patterns of X-rays in a lattice plane with a regular arrangement of atoms in the sample. **Figure 3.1** shows the X-ray diffraction (XRD) results for the synthesized $Zn_3(BO_3)_2$, $Zn_3(BO_3)_2$@C, $Zn_3(BO_3)_2$@LATP, and $Zn_3(BO_3)_2$@C_LATP samples. All four samples, with and without coating, have the same overall phase as the reference peak of $Zn_3(BO_3)_2$. However, the two samples coated with LATP, $Zn_3(BO_3)_2$@LATP and $Zn_3(BO_3)_2$@C_LATP, exhibited a new peak at around 30°, which was attributed to LATP. The peaks represented by an asterisk (*). These peaks are attributed to LATP, confirming its presence, albeit in small quantities.

It is evident that the four synthesized samples have shapes that differ slightly from the $Zn_3(BO_3)_2$ reference peak (ICSD) near 31-38°, as highlighted by the yellow box in **Figure 3.1**. For a detailed comparison, the peak of bare $Zn_3(BO_3)_2$ near 31-38° in **Figure 3.2** was enlarged and compared with the peaks of reference $Zn_3(BO_3)_2$ and ZnO. The synthesized material has a slightly different graph due to the presence of a small amount of ZnO, which is an impurity created during the synthesis process. Although $Zn_3(BO_3)_2$ is converted to some ZnO during battery cycling, the trace impurities of ZnO created during synthesis do not significantly impact the overall performance.[42]

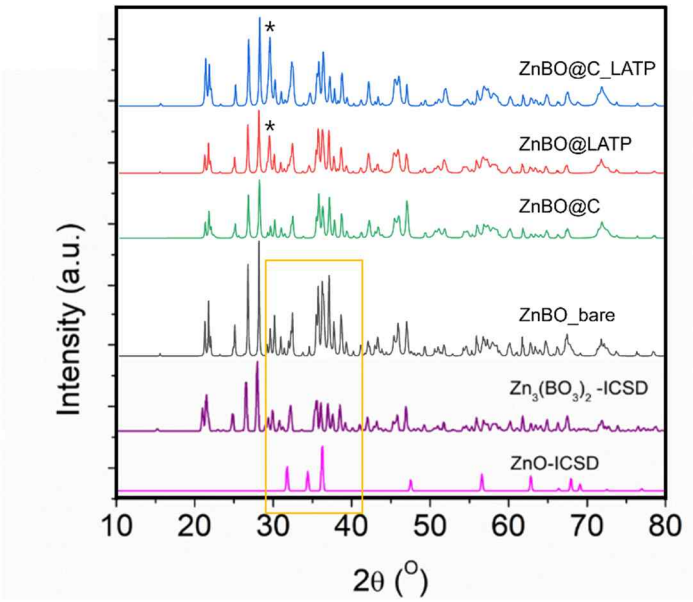

Figure 3.1 The XRD patterns of $Zn_3(BO_3)_2$, $Zn_3(BO_3)_2$@C, $Zn_3(BO_3)_2$@LATP, and $Zn_3(BO_3)_2$@C_LATP.

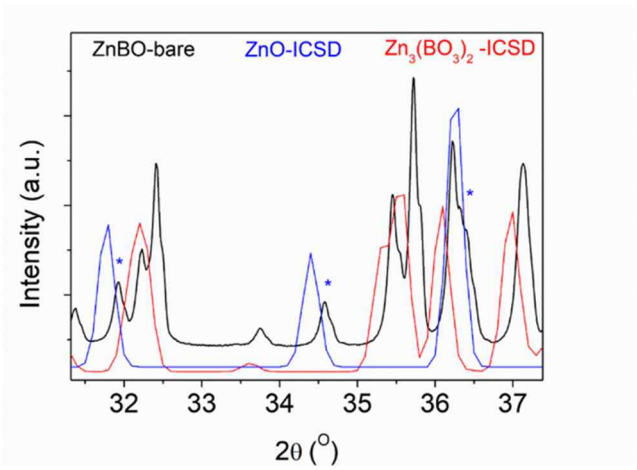

Figure 3.2 The XRD patterns of $Zn_3(BO_3)_2$_bare, ZnO_ICSD, and $Zn_3(BO_3)_2$_ICSD form 31 to 38°.

3.1.2 Field emission scanning electron microscopy and energy dispersie X-ray spectroscopy (FE-SEM/EDX)

Figure 3.3 (a) shows the SEM image of $Zn_3(BO_3)_2$@C_LATP. Only the sample with coating was presented to confirm the success of the coating since there was no significant change in particle size between the coated and uncoated samples. It is important to note that the particle size was not uniform, which is a limitation of the solid-state reaction synthesis method.

The EDX elemental mapping images from **Figure 3.3 (a)** are presented in **Figure 3.2 (b-g)**. **Figure 3.2 (d)** and **(f)** confirm the presence of $Zn_3(BO_3)_2$ due to the uniform distribution of zinc and boron. Additionally, **Figure 3.2 (c)** confirms that the carbon is well coated. In contrast, Ti shows less distribution compared to the other elements in **Figure 3.2 (e)**, indicating a non-uniform distribution of the LATP. It appears to be partially agglomerated, suggesting local presence.

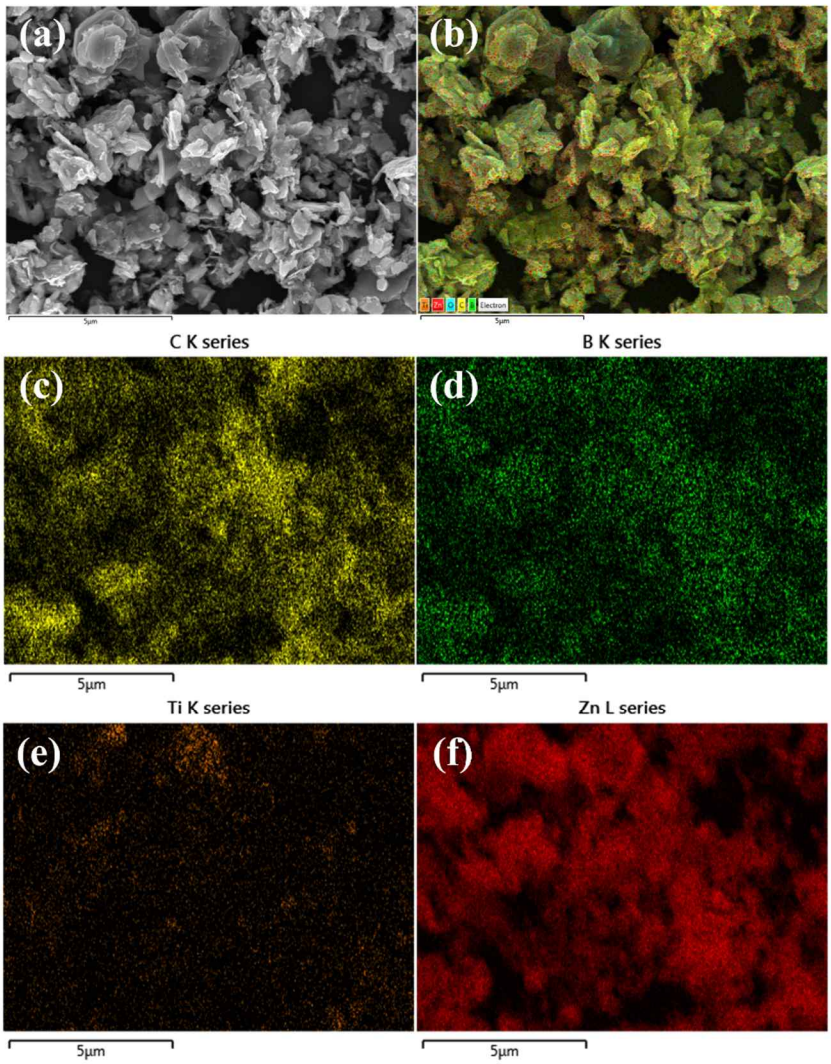

Figure 3.3 (a) SEM and its element mapping images of Zn3(BO3)2@C_LATP for (b) sum of all elements, (c) C, (d) B, (e) Ti, and (f) Zn.

3.2 Electrochemical performance

3.2.1 Cyclic voltammetry

Figure 3.4 (a) shows the cyclic voltammetry (CV) curves for the first and second cycles of the $Zn_3(BO_3)_2$_bare material at a scan rate of 0.05 mV s^{-1}. In the initial cycle of the conversion anode, the liquid electrolyte typically degrades in the sub 1 V region. The electrolyte's $LiPF_6$ decomposes into LiF, which constitutes the majority of the SEI layer. As a result, the anode material's surface is coated with the SEI layer. In that interval, the first and second cycles exhibit different shapes due to these processes. Therefore, it is crucial to analyze the more stable second cycle data. **Figure 3.4 (b)** compares the data for the four synthesized materials, all of which have the same shape.

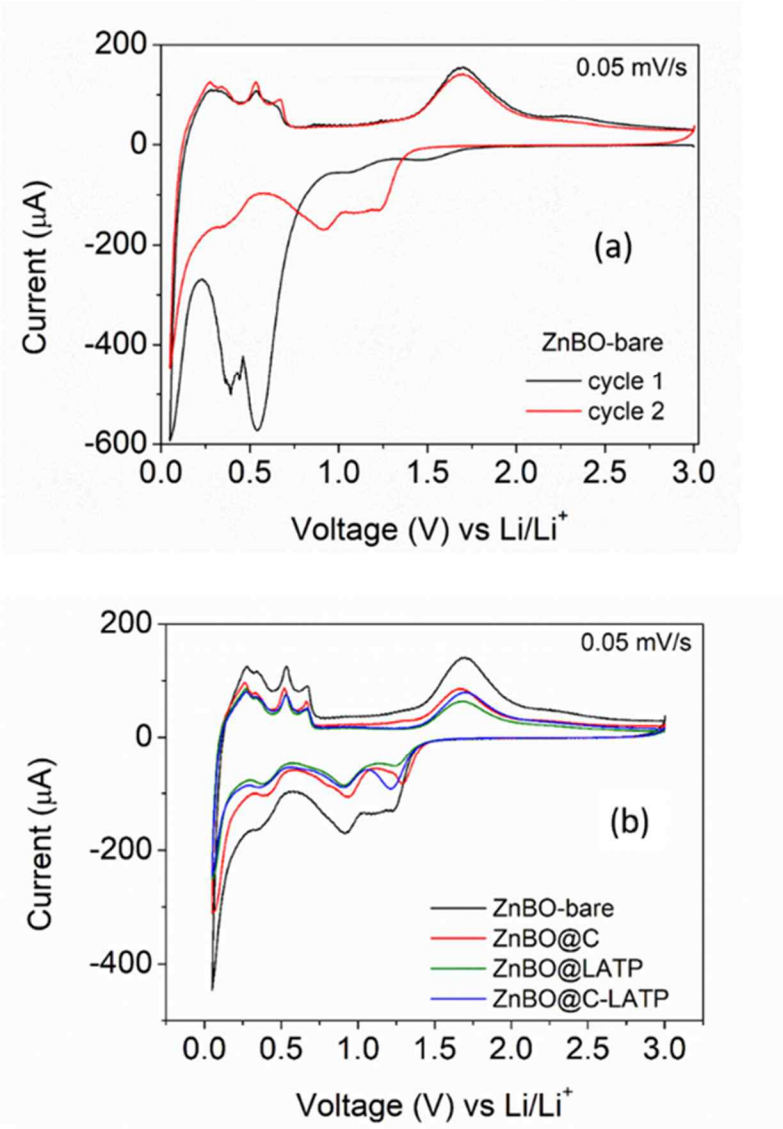

Figure 3.4 (a) CV scans for Zn3(BO3)2 at 1st and 2nd cycle

(b) CV scans for synthesized samples at 2nd cycle.

3.2.2 Charge-discharge curves

Figure 3.5 shows the charge-discharge curves for the initial discharge and 1st cycle of the four samples. At a current density of 0.05 A g^{-1}, the specific capacities of $Zn_3(BO_3)_2$, $Zn_3(BO_3)_2$@C, $Zn_3(BO_3)_2$@LATP, and $Zn_3(BO_3)_2$@C_LATP are 1230.97, 1056.02, 1030.77, and 685.02 mAh g^{-1}, respectively. All samples show irreversible capacity degradation in subsequent cycles, which is a common phenomenon observed in convertible cathodes. Possible reasons for the results include the formation of SEI, side reactions in the electrolyte, and amorphization of the cathode material. The $Zn_3(BO_3)_2$ sample exhibited a reversible discharge capacty of approximately 606.70 mAh g^{-1} at a current density of 0.05 mA g^{-1}, indicating its potential for energy storage applications.

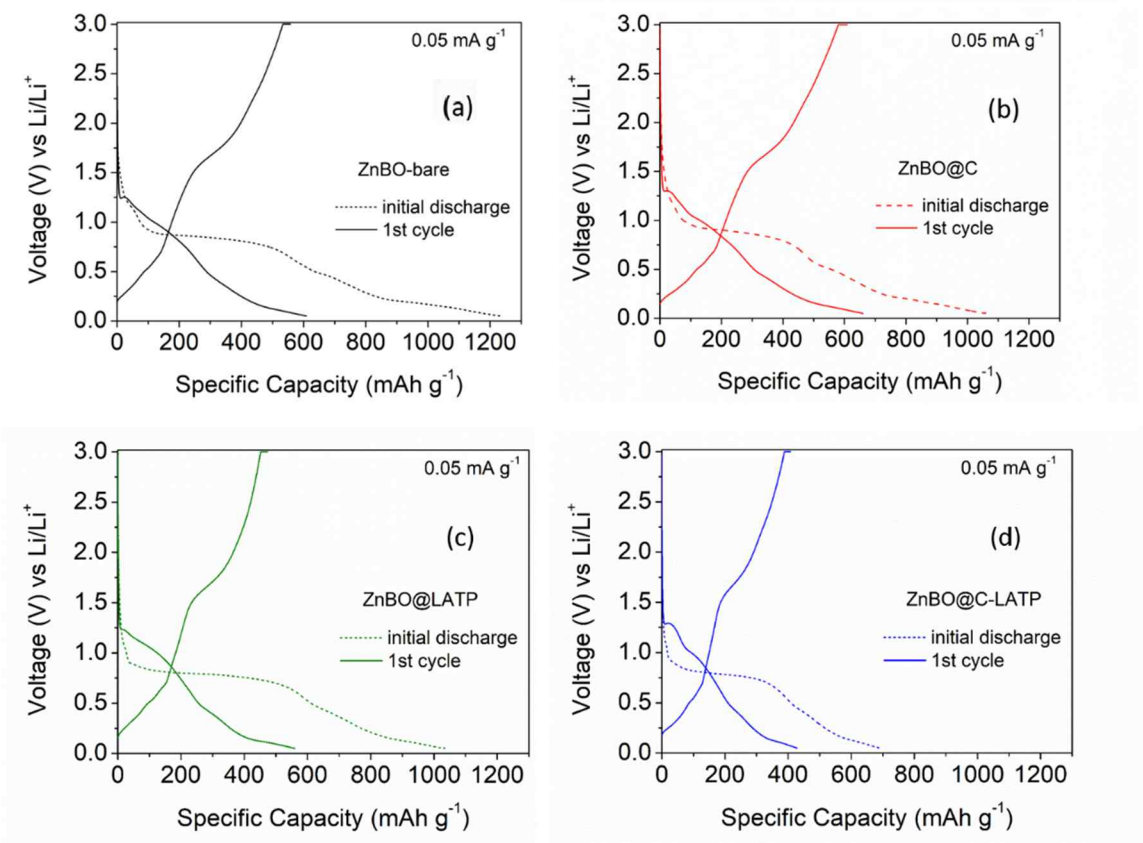

Figure 3.5 Comparison of discharge curves for initial lithiation and charge-discharge curves for the first cycle for samples: (a) $Zn_3(BO_3)_2$, (b) $Zn_3(BO_3)_2$@C, (c) $Zn_3(BO_3)_2$@LATP, and (d) $Zn_3(BO_3)_2$@C_LATP.

3.2.3 Rate performance

The rate performance results for the four samples synthesized are shown in **Figure 3.6**. The cells underwent testing at different C-rates, ranging from 0.05 to 2 A g^{-1}, at a voltage of 0.05 to 3 V, with 3 cycles for each C-rate. The discharge capacity of all samples decreased as the current density increased. Based on the results, $Zn_3(BO_3)_2$@C exhibited the highest capacity. The sample $Zn_3(BO_3)_2$@C exhibits reversible discharge capacities of 673.93, 496.97, 452.88, 417.36, 388.41, 376.76, 352.23, and 309.05 mAh g^{-1} at current densities of 0.05, 0.1, 0.2, 0.3, 0.4, 0.5, 1, and 2 A g^{-1}. At a current density of 0.1 A g^{-1}, the capacity was recovered up to 488.35 mAh g^{-1}, which is similar to the initial capacity of 496.97 mAh g^{-1}, indicating a good capacity recovery rate.

The effect of LATP was investigated by comparing $Zn_3(BO_3)_2$@LATP and $Zn_3(BO_3)_2$@C_LATP. The hybrid coated material performed better with increasing current density. Anode materials must withstand fast charge and discharge rates. We also compared the long cycling of $Zn_3(BO_3)_2$@C, which showed good results overall, and $Zn_3(BO_3)_2$@C_LATP, which performed better among the LATP coated materials.

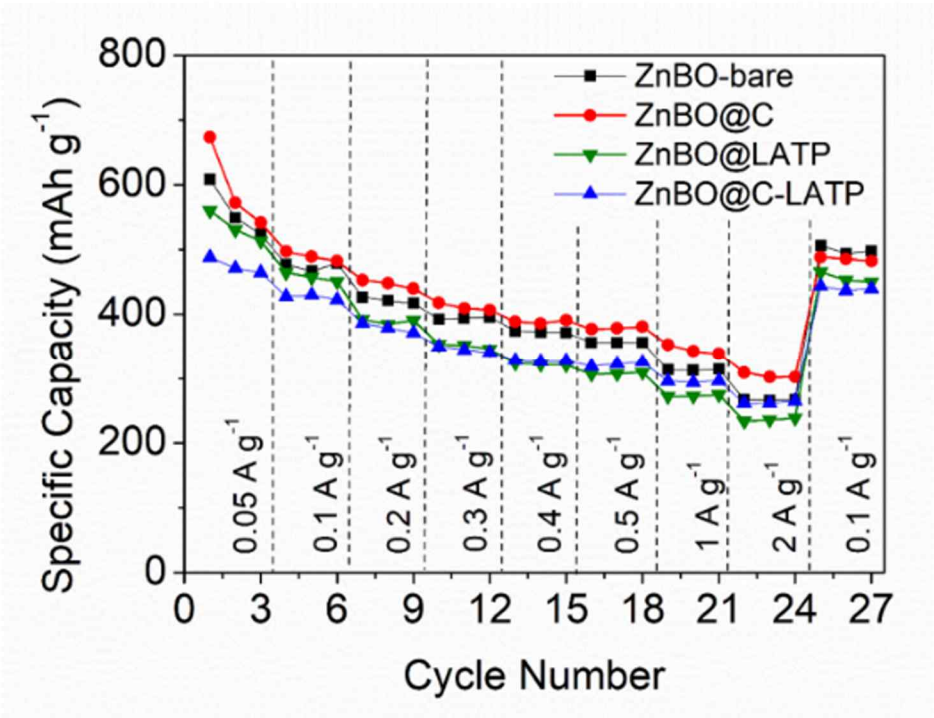

Figure 3.6 Specific discharge capacities of the synthesized samples at different C-rates.

3.2.4 Long cycling performance and dQ/dV

The results of long cycling up to 800 cycles at a rate of 1 A g^{-1} for the two aforementioned samples are shown in **Fig. 3.7**. Both samples show an increasing capacity from the beginning until the 400th cycle, after which it tends to decrease sharply. The initial increase in capacity is due to the SEI formation. At 400th cycles, $Zn_3(BO_3)_2$@C exhibited a maximum capacity of 500.63 mAh g^{-1}, and $Zn_3(BO_3)_2$@C_LATP exhibited a maximum capacity of 470.80 mAh g^{-1}. Afterward, the SEI layer starts to decompose and the degradation is rapid, hence the rapid loss of capacity after 400 cycles.

To further explore this process, we measured dQ/dV plots. **Figure 3.8 (a)** shows that the performance is more stable at the 400th cycle than at the second cycle and decreases from 600 to 800 cycles, which supports the results of long cyclability. Similarly, **Figure 3.8 (b)** shows the results for the hybrid coated samples, where the same trend can be observed, but with less degradation in performance. Since the anode material focuses on charge rate and lifetime, it can be concluded that the $Zn_3(BO_3)_2$@C_LATP exhibits the best performance.

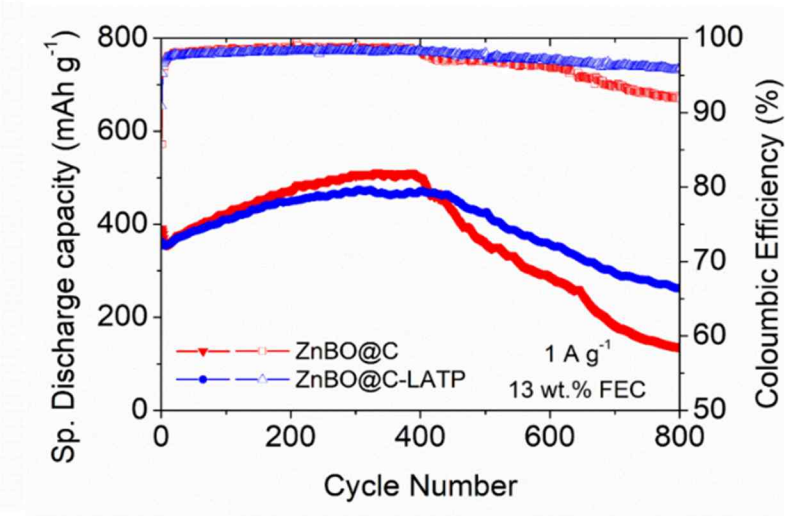

Figure. 3.7 Long cyclability test at a high C-rate of 1 A g-1 for $Zn_3(BO_3)_2$@C and $Zn_3(BO_3)_2$@C_LATP.

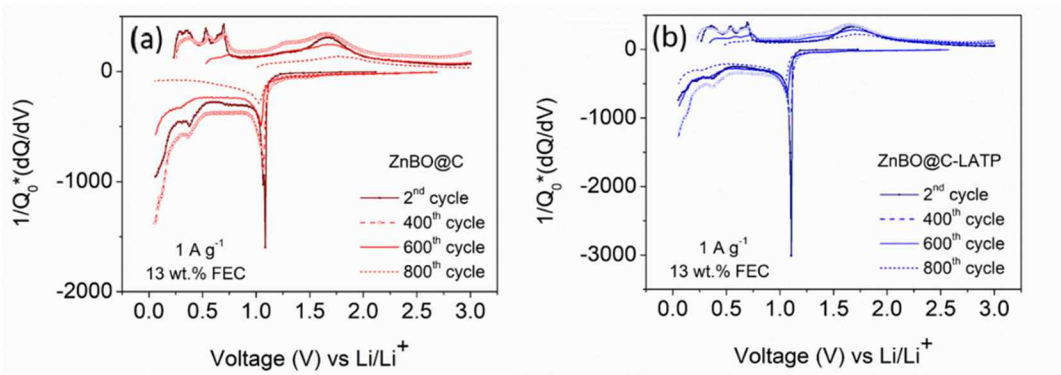

Figure. 3.8 The dQ/dV plot for the different cycles for (a) $Zn_3(BO_3)_2$@C and (b) $Zn_3(BO_3)_2$@C_LATP.

3.2.5 High rate performance

Based on the previous results, we evaluated the performance of the $Zn_3(BO_3)_2$@C_LATP sample, which is expected to have advantages in charge rate and lifetime. We conducted tests at higher C-rates (2, 5, and 10 A g^{-1}) compared to conventional cycling performance. We performed 50 cycles at each C-rate, totaling 150 cycles. During the 150 cycles, the SEI was growing, resulting in a gradual increase in capacity. The maximum capacity observed was 321.24 mAh g^{-1} at a rate of 2 A g^{-1}, 268.40 mAh g^{-1} at 5 A g^{-1}, and 211.09 mAh g^{-1} at the highest rate of 10 A g^{-1}. The anode material demonstrated the ability to maintain a high capacity of approximately 200 mAh g^{-1} at 10 A g^{-1}. This indicates its suitability for high rate cycling.

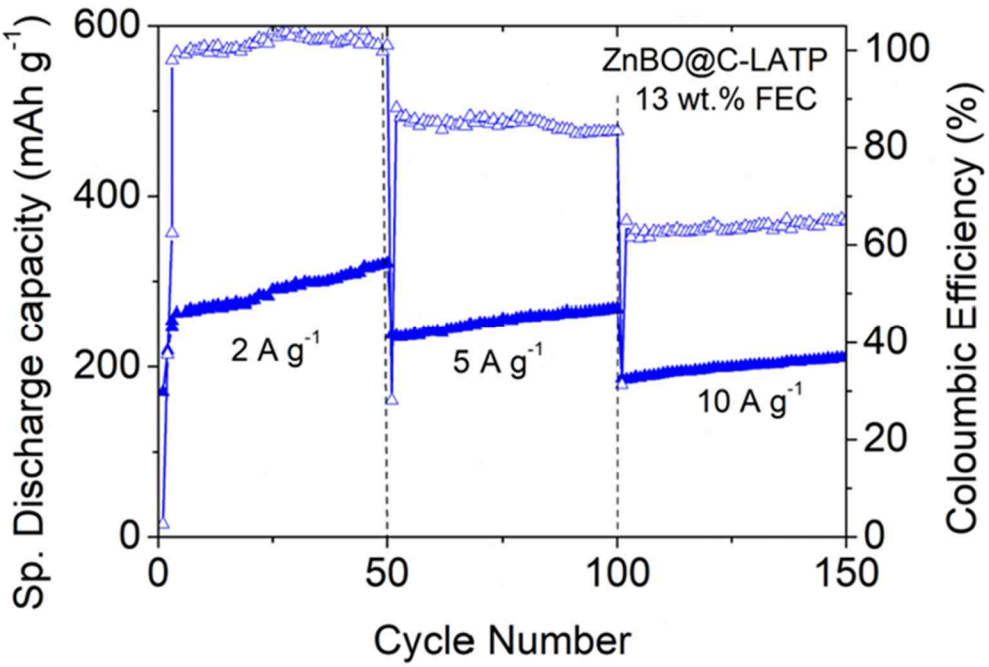

Figure 3.9 Specific discharge capacities of $Zn_3(BO_3)_2$@C_LATP at different high C-rates.

4. Conclusion

$Zn_3(BO_3)_2$ was synthesized using a solid-state reaction method and then coated with C and LATP in two steps to be used as an anode material for lithium-ion batteries. The XRD analysis confirmed successful synthesis of $Zn_3(BO_3)_2$ and identified the peak of LATP. Structural and morphological characterization through SEM-EDX also confirmed successful coating of C and LATP.

$Zn_3(BO_3)_2$@C exhibited the best overall rate performance. In a cycling test lasting up to 800 cycles at a current rate of 1 A g^{-1}, $Zn_3(BO_3)_2$@C_LATP exhibited the best performance. Additionally, the hybrid coated material maintained a stable capacity even at a high charge rate of 10 A g^{-1}. These results suggest that $Zn_3(BO_3)_2$@C_LATP has potential as a cathode material for LIBs.

5. References

1. Reddy, T.B., *Linden's handbook of batteries*. 2011: McGraw-Hill Education.
2. Patrício, J., Y. Kalmykova, P.E. Berg, L. Rosado, and H. Åberg, Waste Management, 2015. 39: p. 236-245.
3. Crompton, T.R., T.P. Crompton, and T.R. Crompton, Battery reference book. 2000: Newnes.
4. Kim, J.Y., D.O. Shin, K.M. Kim, J. Oh, J. Kim, S.H. Kang, M.J. Lee, and Y.-G. Lee, Scientific reports, 2019. 9(1): p. 1-7.
5. Ding, Y., Z.P. Cano, A. Yu, J. Lu, and Z. Chen, Electrochemical Energy Reviews, 2019. 2(1): p. 1-28.
6. Fan, X., B. Liu, J. Liu, J. Ding, X. Han, Y. Deng, X. Lv, Y. Xie, B. Chen, and W. Hu, Transactions of Tianjin University, 2020. 26(2): p. 92-103.
7. Köhler, U., J. Kümpers, and M. Ullrich, Journal of power sources, 2002. 105(2): p. 139-144.
8. YANG, Zhuo, et al. Rechargeable sodium-based hybrid metal-ion batteries toward advanced energy storage. Advanced Functional Materials, 2021, 31.8: 2006457.
9. Pistoia, G. Lithium-Ion Batteries; Elsevier: Amsterdam, The Netherladns, 2013.
10. T. Horiba, K. Hironaka, M. Matsumura, et al., J. Power Sources, 2001, 97-98, 719.
11. T. Horiba, K. Hironaka, T. Matsumura, T. Kai, M. Koseki, Y. Muranaka, J. Power Sources, 2003, 119–121, 893.
12. LANDI, Brian J., et al. Carbon nanotubes for lithium ion batteries. Energy & Environmental Science, 2009, 2.6: 638-654.
13. MUSLIMIN, Selamat, et al. Comparison of Batteries Used in Electrical Vehicles. In: 5th FIRST T1 T2 2021 International Conference (FIRST-T1-T2 2021). Atlantis Press, 2022. p.

421-425.

14. GOODENOUGH, John B. Rechargeable batteries: challenges old and new. Journal of Solid State Electrochemistry, 2012, 16: 2019-2029.

15. HAUSBRAND, R., et al. Fundamental degradation mechanisms of layered oxide Li-ion battery cathode materials: Methodology, insights and novel approaches. Materials Science and Engineering: B, 2015, 192: 3-25.

16. Whittingham, M. S., Lithium Batteries and Cathode Materials. Chemical Reviews 2004, 104 (10), 4271-4302.

17. Heide Budde-Meiwes, J. D., Benedikt Lunz, Jens Muennix, Susanne Rothgang, Julia Kowal and Dirk Uwe Sauer, A review of current automotive battery technology and future prospects. J Automobile Engineering, 2013, 227 (5), 761-776.

18. R. Koksbang, J. Barker, H. Shi, M. Saidi, Solid State Ionics, 1996, 84,1-21.

19. K. Y. Lee, H. H. Byeon, C. Jang, J. H. Choi, I. S. Choi, Y. Jung, W. Kim, J. Chang and H. Yi, *Adv. Mater*, 2015, *27*, 922.

20. HU, Jingwei; ZHONG, Shengwen; YAN, Tingting. Using carbon black to facilitate fast charging in lithium-ion batteries. Journal of Power Sources, 2021, 508: 230342.

21. H. Gwon, D.-H. Seo, S. W. Kim, J. Kim, and K. Kang, Adv. *Funct. Mater*, 2009, *19*, 3285.

22. CHEN, Jun, et al. Microcrystalline copper foil as a high performance collector for lithium-ion batteries. Journal of Power Sources, 2019, 438: 226973.

23. XIE, Lijing, et al. Hard carbon anodes for next-generation Li-ion batteries: review and perspective. Advanced Energy Materials, 2021, 11.38: 2101650.

24. MONEM, Mohamed Abdel, et al. Lithium-ion batteries: Evaluation study of different charging methodologies based on aging process. Applied Energy, 2015, 152: 143-155.

25. MA, Canliang, et al. Synthesis and electrochemical properties of artificial graphite as an anode for high-performance lithium-ion batteries. Carbon, 2013, 64: 553-556.

26. GALLEGO, Nidia C., et al. Advanced surface and microstructural characterization of natural graphite anodes for lithium ion batteries. Carbon, 2014, 72: 393-401.

27. XIE, Lijing, et al. Hard carbon anodes for next-generation Li-ion batteries: review and perspective. Advanced Energy Materials, 2021, 11.38: 2101650.

28. JIN, Yan, et al. Challenges and recent progress in the development of Si anodes for lithium-ion battery. Advanced Energy Materials, 2017, 7.23: 1700715.

29. GATTU, Bharat. A Fundamental Study of Nanostructured Si Anodes for Lithium Ion Batteries. 2020. PhD Thesis. University of Pittsburgh.

30. NZEREOGU, P. U., et al. Anode materials for lithium-ion batteries: A review. Applied Surface Science Advances, 2022, 9: 100233.

31. AN, Seong Jin, et al. The state of understanding of the lithium-ion-battery graphite solid electrolyte interphase (SEI) and its relationship to formation cycling. Carbon, 2016, 105: 52-76.

32. LEE, Lanlee, et al. Self-adaptive anode design with graphene-coated SiOx/graphite for high-energy Li-ion batteries. Chemical Engineering Journal, 2022, 442: 136166.

33. LINDGREN, Fredrik, et al. SEI formation and interfacial stability of a Si electrode in a LiTDI-salt based electrolyte with FEC and VC additives for Li-ion batteries. ACS applied materials & interfaces, 2016, 8.24: 15758-15766.

34. ZHENG, Jianming, et al. Research progress towards understanding the unique interfaces between concentrated electrolytes and electrodes for energy storage applications. Advanced Science, 2017, 4.8: 1700032.

35. SU, Chi-Cheung, et al. Cyclic carbonate for highly stable cycling of high voltage lithium

metal batteries. Energy Storage Materials, 2019, 17: 284-292.

36. BOMMIER, Clement, et al. New paradigms on the nature of solid electrolyte interphase formation and capacity fading of hard carbon anodes in Na-ion batteries. Advanced Materials Interfaces, 2016, 3.19: 1600449.

37. HOU, Tingzheng, et al. The influence of FEC on the solvation structure and reduction reaction of LiPF6/EC electrolytes and its implication for solid electrolyte interphase formation. Nano Energy, 2019, 64: 103881.

38. PYUN, Su-Il. Compositional analysis of passivating surface film formed on carbon electrode in organic electrolytic solution using in-situ spectroelectrochemical technique. Metals and Materials, 1999, 5: 101-108.

39. TAKADA, Koji; YAMADA, Yuki; YAMADA, Atsuo. Optimized nonflammable concentrated electrolytes by introducing a low-dielectric diluent. ACS applied materials & interfaces, 2019, 11.39: 35770-35776.

40. YAMADA, Yuki. Developing new functionalities of superconcentrated electrolytes for lithium-ion batteries. Electrochemistry, 2017, 85.9: 559-565.

41. HUANG, Lin-Bo, et al. trans-Difluoroethylene Carbonate as an Electrolyte Additive for Microsized SiO x@ C Anodes. ACS Applied Materials & Interfaces, 2021, 13.21: 24916-24924.

42. WANG, Sai; ZHANG, Xin-Bo. N-doped C@ Zn3B2O6 as a low cost and environmentally friendly anode material for Na-ion batteries: high performance and new reaction mechanism. Advanced Materials, 2019, 31.5: 1805432.